Lizarralde, D., et al., 2023, Carbon released by sill intrusion into young sediments measured through scientific drilling: Geology, https://doi.org/10.1130/G50665.1

SUPPLEMENTARY MATERIAL

Carbon release due to sill intrusion into sediments measured through scientific drilling

Daniel Lizarralde[1], Andreas Teske[2], Tobias W. Höfig[3], Antonio González-Fernández[4], and the IODP Expedition 385 Scientists*

IODP Expedition 385 Scientists (alphabetical order)

Ivano W. Aiello[5], Jeanine L. Ash[6], Diana P. Bojanova[7], Martine D. Buatier[8], Virginia P. Edgcomb[1], Christophe Y. Galerne[9], Swanne Gontharet[10], Verena B. Heuer[11], Shijun Jiang[12], Myriam A.C. Kars[3], Ji-Hoon Kim[13], Louise M.T. Koornneef[14], Kathleen M. Marsaglia[15], Nicolette R. Meyer[16], Yuki Morono[17], Raquel Negrete-Aranda[4], Florian Neumann[4], Lucie C. Pastor[18], Manet E. Peña-Salinas[19], Ligia L. Pérez Cruz[20], Lihuan Ran[21], Armelle Riboulleau[22], John A. Sarao[23], Florian Schubert[24], S. Khogenkumar Singh[25], Joann M. Stock[26], Laurent M.A.A. Toffin[27], Wei Xie[28], Toshiro Yamanaka[29], and Guangchao Zhuang[30]

[1]Dept. of Geology and Geophysics, Woods Hole Oceanographic Institution, Woods Hole MA 02543, USA

[2]Dept. of Earth, Marine and Environmental Sciences, University of North Carolina at Chapel Hill, CB 3300, Chapel Hill NC 27599, USA

[3]International Ocean Discovery Program, Texas A&M University, 1000 Discovery Drive, College Station TX 77845, USA

[4]Dept. of Geology, CICESE, 3918 Carretera Ensenada-Tijuana, Zona Playitas, Ensenada BC 22860, Mexico

[5]Dept. of Geological Oceanography, Moss Landing Marine Laboratories, 8272 Moss Landing Road, Moss Landing CA 95039-9647, USA

[6]Dept. of Earth, Environmental and Planetary Sciences, Rice University, 6100 Main Street MS-126, Houston TX 77005, USA,

[7]Dept. of Earth Sciences, University of Southern California, 825 Bloom Walk ACB 302, Los Angeles CA 90034, USA

[8]UMR Chrono-Environnement, Université Bourgogne Franche-Comté, 16 Route de Gray, 25030 Besancon, France

[9]Forschungsgruppe “Petrologie der Ozeankruste”, Fachbereich Geowissenschaften, Universität Bremen, Germany

[10]Laboratoire d'Océanographie et du Climat: Expérimentations et Approches Numériques, Sorbonne Université, Campus Pierre et Marie Curie, France

[11]Dept. of Geosciences, University of Bremen, Leobener Strasse 8, 28359 Bremen, Germany

[12]Institute of Groundwater and Earth Sciences, Jinan University, 601 West Huangpu Dadao, Guangzhou GD 510632, China

[13]Petroleum and Marine Research Division, Korea Institute of Geoscience & Mineral Resources (KIGAM), 124 Gwahak-ro Yuseoug-gu, Daejeon 305-350, Republic of Korea

[14]Earth and Environmental Sciences, School of Geography, University of Plymouth, Drake Circus, Fitzroy Building 306, Plymouth, Devon PL4 8AA, United Kingdom

[15]Dept. of Geological Sciences, California State University, Northridge, 18111 Nordhoff Street, Northridge CA 91330-8266, USA

[16]Dept. of Earth System Science, Stanford University, 367 Panama Street, Stanford CA 94305, USA

[17]Kochi Institute for Core Sample Research, Japan Agency for Marine-Earth Science and Technology, Monobe B200, Nankoku Kochi 783-8502, Japan

[18]Univ. Brest, Biologie et Ecologie des Ecosystems Marns Profonds, CNRS, IFREMER, UMR 6197, Rue Dumont d'Urville, Plouzané, France

[19]Dept. of Coastal Oceanography, UABC, 3917 Carretera Ensenada-Tijuana, Zona Playitas, Ensenada BC 22860, Mexico

[20]Institute of Geophysics, Universidad Nacional Autónoma de México (UNAM), Circuito Interior de Cd. Universitaria SN. Coyoacan, Mexico City 04510, Mexico

[21]The Second Institute of Oceanography, Ministry of Natural Resources, Laboratory of Marine Ecosystem and Biogeochemistry, 36 Baochu Bei Road, Hangzhou, China

[22]Laboratoire d'Océanologie et de Géosciences, Université de Lille, Lille 1 Sciences et Technologies, Bâtiment SN5, Cedex 59655 Villeneuve-d'Asq, France

[23]College of Geosciences, Texas A&M University, 3115 TAMU, College Station TX 77843, USA

[24]Section Geomicrobiology, GFZ (German Research Centre for Geosciences), Helmholtz Centre Potsdam, Telegrafenberg, 14473 Potsdam, Germany

[25]CSIR-National Institute of Oceanography, Council of Scientific & Industrial Research (CSIR), Ministry of Science and Technology, India

[26]Division of Geological and Planetary Sciences, California Institute of Technology, 1200 E. California Boulevard, Pasadena CA 91125, USA

[27] Univ Brest, Laboratoire de Microbiologie des Environnements Extrêmes LM2E, CNRS, IFREMER, UMR 6197, IUEM, Rue Dumont d'Urville, F-29280 Plouzané, France

[28]College of Oceanography, Hohai University, 1 Xikang Street, Gulou District, Nanjing, China

[29]Dept. of Ocean and Environmental Sciences, Tokyo University of Marine Science and Technology, 4-5-7 Konan Minato-ku, Tokyo 108-8477, Japan

[30]Key Laboratory of Marine Chemistry and Technology, Ocean University of China, China

Sulfate and Methane at IODP Sites U1545 and U15456

The majority of the supplementary material in this Repository involves a description of the stratigraphic correlation between IODP Expedition 385 drill Sites U1545 and U1546. We also include here a figure, referenced in the main text, of measurements of pore water sulfate and core-headspace measurements of methane concentration. We present this figure first, since it is not directly related to the description of stratigraphic correlation.

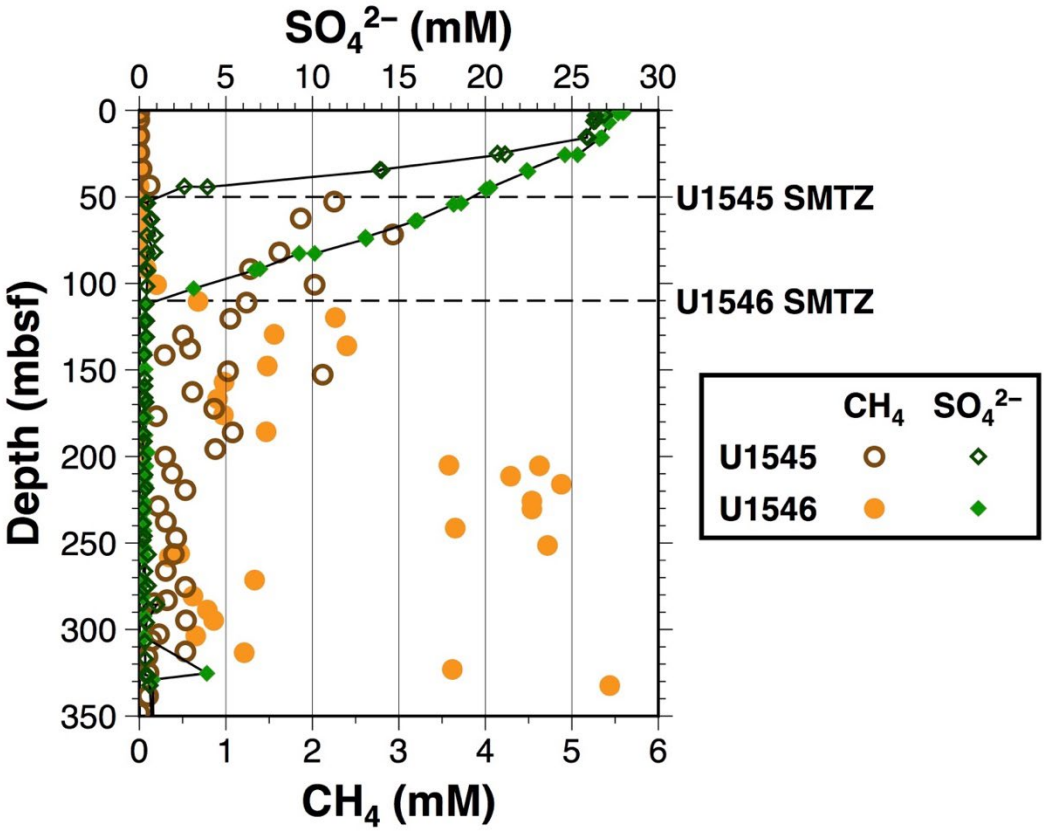

Figure S1. *Sulfate and Methane.* Sulfate from porewater measurements and methane concentrations measured from head-space gas samples for both Sites U1545 and U1546. The indicated sulfate/methane transition zone (SMTZ) for each site is based on sulfate and other measured porewater compounds.

Stratigraphic Correlation

A hallmark contribution of this paper is the comparison of *in situ* samples and measurements from closely located and well correlated borehole sites – one impacted by igneous sill intrusion (Site U1546) and one un-impacted (Site U1545), in order to estimate organic carbon loss from sediments in response to sill intrusion. We describe here the stratigraphic correlation between IODP Expedition 385 drill Sites U1545 and U1546 that enables the estimation of carbon loss. Three holes were drilled and cored at each Site, and Holes U1545A and U1546C were also logged with Schlumberger logging tools. We use stratigraphy delineated by the multi-channel seismic data, sedimentological descriptions of cores, and the *in situ* natural gamma ray logs from the downhole logging runs to correlate strata and samples between Sites U1545 and U1546.

The depth migrated seismic data are an integral component of the site-to-site correlation, and so we first provide a brief description of how those data were migrated.

The correlation of pre-intrusion strata between Sites U1545 and U1546 is impacted by three main factors: 1) lateral non-uniformity of strata prior to sill intrusion, 2) disruption due to sill intrusion, including structural disruption to sediments at Site U1546 and offsetting of sediments that had previously been laterally continuous between Sites U1545 and U1546, and 3) deformation of the seafloor due to the sill intrusion, resulting in laterally non-uniform post-intrusion sedimentation across the two Sites. We consider these factors in the order (3), (1), and then (2). The 'Stratigraphic Correlation' portion of this appendix is organized into five sections identified with bold paragraph headings as:

Depth migration

Post-intrusion stratigraphy

Lateral stratal variations prior to sill intrusion

Disruptions due to the sill intrusion

Site-to-Site Correlation between Sites U1545 and U1546

Noteworthy features in the density logs

Depth migration. Stacked and migrated multi-channel seismic (MCS) data provide vertical records, or traces, of seismic impedance contrasts with two-way travel time. The lateral spacing of those traces is small relative to the wavelength of the vertical signals, and so a seismic section, consisting of sequences of traces, provides images of laterally continuous strata as well as features that disrupt that lateral continuity. These data are most useful when presented with depth rather than travel time as the vertical axis. The conversion from time to depth requires an accurate velocity model. Sonic velocity logs at Sites U1545 and U1546 provide high-resolution (i.e. at wavelengths of velocity variation that are smaller than corresponding wavelengths of the seismic data) measurements of seismic velocity with depth. We use these to create a 2D velocity model which is in turn used to migrate the MCS data to depth. The resulting depth-migrated seismic data provide very accurate images of seismic impedance with depth at the individual drill-site locations, and it is this accuracy that is most relevant to the correlation. The depth accuracy of impedance contrasts away from the drill sites depends on the interpolation of velocity away from those sites, and so we describe that here.

We constructed a 2D velocity model from the velocity logs by assuming that velocity varies linearly along correlative boundaries between sites. We use boundaries identified in the time-migrated seismic data, indicated in Figure S2 in depth, to translate velocity laterally above boundary '3' between sites using a linear interpolation, and the velocities from Sites U1545 and U1546 were translated northwest and southeast, respectively, using those same boundaries. Below boundary '3', we picked surfaces from the time-migrated seismic data for the top and bottom of the observed sill. Velocity logs converted to depth provide an accurate depth assignment to features observed in time seismic section, and so the sill top and bottom reflectors were confidently picked at Site U1546 and translated laterally in a straightforward way. Those top and bottom sill surfaces meet at a point approximately half-way in between the two sites. The upper surface was used to interpolate sediment velocities between the two sites, and similarly for the bottom surface.

The velocity model resulting from the interpolation of the sonic log velocities along boundaries between sites, and from projecting those velocities along the same boundaries

away from sites, was used to migrate the stacked MCS data using a split-step frequency/wavenumber migration approach (Stoffa et al., 1990; Kessinger and Stoffa, 1992; Lizarralde and Holbrook, 1997).

Post-intrusion stratigraphy. We aim to compare sediments that were known to be present at the time of the sill-intrusion event. We thus want to distinguish pre- and post-intrusion sediments. Seismic stratigraphy indicates greater post-intrusion sediment deposition over Site U1545 relative to Site U1546. Three seismic sequence boundaries, which we refer to as B1, B2 and B3, are noted in Figure S2 as circled 1, 2 and 3. Along with the seafloor, those boundaries define three layers, which we refer to as Layer 1, Layer 2 and Layer 3. The deepest boundary (B3, labeled 3 in Figure S1a) marks substantial unconformities (e.g. 'U' in Figure S2b) between Layer 3 strata and those beneath the boundary, where the strata are clearly deformed (including brittle deformation) in the region above the sill intrusion. It is thus tempting to assume that B3 marks the paleo-seafloor at the time of the intrusion. However, the thickness of Layer 3 is similar at Sites U1545 and U1546 (numbers in Figure S2a), and the seismic character of Layer-3 strata is laterally variable and in places chaotic. It is possible that Layer 3 was present at the time of intrusion and, at that time, B3 separated strata with different strength properties. In that case, uplift of deformed, stiffer sediments beneath B3 may have driven viscous deformation within Layer 3 sediments.

Substantial later variation in sediment thickness is observed in Layer 2, which is 50 m thick at Site U1546 and 77 m thick at Site U1545. The seismic stratigraphy indicates that this difference is related to sediment accumulation (noted by 'B' in Figure S2b) in a seafloor depression beneath Site U1545. Core data from Site U1545 indicate slump deposits within this interval. It is plausible that this depression formed in response to sill intrusion. The stratigraphy suggests that the surface indicated as 'Y' in Figure S2b is the youngest likely syn-intrusion paleo surface, with B3 being the oldest likely syn-intrusion paleo surface. Seafloor topography created by sill intrusion continues to be diminished by ongoing laterally variable deposition. For example, a wedge of sediment thickening from Site U1546 to Site U1545 in Layer 1 accounts for the 8-m difference in Layer-1 sediment thickness between the two Sites.

Lateral stratal variations prior to sill intrusion. Given the uncertain identification of a particular paleo surface marking sill intrusion, we consider sediments below B3 for the site-to-site comparison of sedimentary organic carbon and thus focus our stratigraphic correlation on those sediments. All of that section for Site U1545 and most for Site U1546 is shown in the enlarged panel of Figure S2b. It is clear in the enlarged panel that there is a characteristic pattern to the sequence of seismic reflectors that can be visually correlated from Site U1545 to U1546. These individual units have thicknesses that vary slightly from site to site, but they were almost certainly continuous between the sites prior to the sill-intrusion event. The sole exception to this lateral stratal continuity that we have identified is the sedimentary 'wedge' indicated by blue arrows in Figure S3b. This interval downlaps onto a mostly horizontal surface at ~1.947 meters depth and is absent at Site U1545 but present at ~13-m thickness at Site U1546. The curvature of strata overlying the wedge between Site U1545 and the location marked by the dashed line and labeled 'M' in Figure S3b is very likely due to the presence of the wedge and not related to the emplacement of the sill.

The correlation of the 'wedge' strata between position 'M' and Site U1546 is shown in Figure S4, where the seismic data are tied at the wedge boundary. The correlation is strong, suggesting that the wedge layer maintained a near constant thickness between 'M' and Site U1546. The 'pattern' of correlation of overlying strata is also evident in this figure, and the growing offset of correlative strata away from the wedge tie points is indicative of lateral variability of individual layer thicknesses.

The absence of 'wedge' sediments at Site U1545 and their presence at Site U1546 means that there are no core samples from Site U1545 that are correlative to samples taken from Site U1546 over the wedge interval, i.e. there is a gap in the correlation between the two sites. This gap is illustrated in Figure S5b, a seismic alignment of Sites U1545 and U1546 tied at the top wedge boundary. Also note that the visual correlation of strata between Sites U1545 and U1546 below the wedge interval is improved in Figure S4b, where the gap in correlative strata is accounted for at Site U1545, relative to Figure S4a, where the gap has not been accounted for.

Disruption due to sill intrusion. Figure S2a demonstrates substantial sedimentary disruption above the intruded sill. However, Site U1546 was chosen because the disruption is minor there, with the primary disruptions due to sill intrusion being vertical uplift of sediments overlying the sill and compaction of sediments underlying the sill. Both of these effects can be confidently accounted for using the natural gamma ray (NGR) logs acquired at each Site, shown in Figure S6. These logs measure naturally occurring gamma-ray radiation emitted from the sediments. Clay rich sediments emit significantly more gamma rays than other types of sediments, and this makes NGR logs ideal for delineating strata in sedimentary successions that are alternately dominated by biogenic and terrigenous sediment. Measured NGR is also sensitive to the density of sediments. For a given stratal unit, NGR counts increase with increasing density because the source elements (uranium, thorium, potassium) are correspondingly more concentrated.

Site-to-Site Correlation between Sites U1545 and U1546. A quick visual inspection of the NGR logs for Sites U1545 and U1546 (Figure S6) reveals numerous notable common signals. The process of correlating strata between the two sites involved matching common signals from one site to the other, and this was done by inspection and in concert with the depth-migrated seismic data. This process is demonstrated in Figure S7 and described in the caption to that figure. The set of 24 tie points plus 2 discontinuities shown in Figure S7 defines the site-to-site correlation used to align the NGR profiles shown in Figure S8, the density profiles shown in Figure S10 and, importantly, to map Site U1545 core samples to correlative depths at Site U1546.

The three main correlative intervals for these two sites, referenced to Site U1546, are 1) the upper interval extending from surface B3 at Site U1546 downward to the top of the 'wedge', 2) from the base of the 'wedge' to the top of the sill, and 3) from the bottom of the sill to the end of useful data on the Site U1545 log. The colored lines in Figure S6 indicate the shifts in depth from the Site U1545 log to the Site U1546 log that align correlative peaks or troughs of the two logs (X-axis scale at the figure's bottom boundary). The shifts for the upper interval, indicated in blue, are approximately 50 m, meaning that correlative features are ~50 m shallower at Site U1546 than at Site U1545 for the upper interval. Variations in shift value with depth reflect

site-to-site differences in the thickness of individual stratal units. The average shift applied to align correlative features over the upper interval is noted, also in blue, as 48.9 m, as is the difference in thickness between the two intervals in percent. The 0% thickness difference for the upper interval indicates that the total thickness of this interval is the same at Site U1546 as at U1545, though thicknesses of individual stratal units within the interval differ from site to site. This same labeling is used for the lower two intervals. For the interval above the sill (green), the decrease in average shift reflects the correlation beneath the sediment 'wedge', which is present at Site U1546 but absent at Site U1545, and the positive 4% thickness reflects the ~1.2m greater thickness of the correlated strata at U1546 relative to U1545. For the bottom interval, the average shift is negative because the correlative sediments at Site U1545 are at a shallower depth than those beneath the sill at Site U1546. The -32% difference in thickness between the lower correlative units at Site U1545 and U1546 is notable. The negative value indicates that that this correlative unit is ~11.4 m thinner at Site U1546 than at Site U1545. We interpret this thickness difference as compression of the sediments underlying the sill due to the weight of the sill. This is consistent with details of the NGR signal and with density measurements from logging, described below.

An expanded view of the correlated NGR logs is shown in Figure S8, with the Site U1546 log shown in brown and the Site U1545 log in black. Visual inspection shows that the correlation at all depths is excellent to very good, including the correlation beneath the sill. The NGR log for Site U1546 has values substantially higher over the lower correlative interval than those for Site U1545 over that interval. The increase in NGR values at U1546 very likely reflects increased density of those sediments due to compaction (e.g., Nobes et al., 1992), with clay-poor intervals exhibiting only minor increases that appear as negative excursions. These diagnostic excursions enable confident, detailed correlation of strata within the indurated and compacted intervals above and below the sill.

The correlation defined by the tie points and discontinuities shown in Figure S7 was used to map the Site U1545 density log to the correlative depths at Site U1546, with the result shown Figure S8. (The same figure is show in condensed form in the main text as Fig. 3b.) As with the NGR, the correlation of features is excellent to very good everywhere data exist. The same

correlative gap noted in the NGR data is present here, due to the presence of a sedimentary wedge at U1546 that does not exist at U1545. In addition, there is a ~170-m interval over which the recording of the wireline density data at U1545 failed. Unfortunately, that interval correlates will sediments directly above the sill at U1546. These two density profiles are used to convert weight percent total organic carbon measured in core sample to volumetric carbon. To fill the gap in the Site U1545 density data above the sill, we chose to use the median of the values that exist over the depth interval spanned by the green line, which is plotted at that median value. We also plot density measured from core samples as blue dots. These are generally consistent with the median value, given the intrinsic variation of density with depth.

Noteworthy features in the density logs. There are several features observed in the density profiles worth noting – these are related to carbonate, silica transformation and induration/compaction.

Carbonate. The large positive excursions noted on both density profiles are almost certainly related to carbonate in most if not all cases. Carbonate formation is a common by product of carbon cycling within the sulfate/methane transition zone (SMTZ), where microbes use sulfate to oxidize methane into bicarbonate. Precipitation of carbonate can occur if sufficient concentrations of bicarbonate and appropriate cations (Ca^{2+} or Mg^{2+}) are present. Numerous dolomitic nodules were recovered in cores from both sites, presumably from layered carbonate (Teske et al., "U1545", 2021; Teske et al., "U1546", 2021). The numerous occurrences of well correlated density peaks throughout these logs tend to suggest that the SMTZ existed at very similar depths at both sites during the period of time prior to sill intrusion. As noted in the main text, the difference in present-day SMTZ depth between the two sites is large.

Silica transformation. Density (Fig. S9) and NGR counts (Fig. S8) each increase abruptly at the correlated depth of 1.918 m at both Sites U1545 and U1546. These increases coincide with the lithologic transition to siliceous claystone accompanying the change in the primary silica phase from opal-A to opal-CT (Teske et al., "U1545", 2021; Teske et al., "U1546", 2021).

Induration/compaction. Average density at Site U1546 increases significantly within the 12-m interval above and a 17-m interval below the sill. These intervals lie within the metamorphic aureole of the sill as defined by source rock analyses (Fig. 3 from main text). Density at Site

U1546 below 2.05 km (i.e. below the lower compacted and indurated zone) remains higher, by ~7%, than correlative density at Site U1545. This may indicate the effects of compaction extending to deeper depths below the sill, which would be expected.

References

Kessinger, W., and P. L. Stoffa, Extended split-step Fourier migration. *Proc. Lnt. Soc. Explor. Geophys.* **62**, 917–918 (1992).

Lizarralde, D., and W. S. Holbrook, U.S. mid-Atlantic margin structure and early thermal evolution. *Journal of Geophysical Research: Solid Earth*, *102*, 22855–22875 (1997).

Nobes, D. C., R. W. Murray, S. Kuramoto, K. A. Pisciotto, and P. Holler, Impact of silica diagenesis on physical property variations, *in* Pisciotto, K. A., Ingle, J. C , Jr., von Breymann, M. T., Barron, J., et al., *Proceedings of the Ocean Drilling Program, Scientific Results,* Vol. 127/128, Pt. 1, (1992).

Stoffa, P. L., J. T. Fokkernat, R. M. de L. Freire, and W.P. Kessinger, W. P., Split-step Fourier migration. *Geophysics* **55**, 410–421 (1990).

Teske, A., D. Lizarralde, T. W. Höfig, the Expedition 385 Scientists, "U1545" in *Proceedings of the International Ocean Discovery Program, Expedition Reports*, Proceedings of the International Ocean Discovery Program., A. Teske, D. Lizarralde, T. W. Höfig, Expedition 385 Scientists, Eds. (International Ocean Discovery Program, 2021).

Teske, A., D. Lizarralde, T. W. Höfig, the Expedition 385 Scientists, "U1546" in *Proceedings of the International Ocean Discovery Program, Expedition Reports*, Proceedings of the International Ocean Discovery Program., A. Teske, D. Lizarralde, T. W. Höfig, Expedition 385 Scientists, Eds. (International Ocean Discovery Program, 2021).

Figure Captions

Figure S2. a) Depth migrated seismic image with locations and total drilled depths of Sites U1545 and U1546 indicated by vertical blue lines. Three seismic sequence boundaries are noted in black with the thickness of the corresponding layers at the two drill sites indicated in meters. Black box indicates the region enlarged in (b). **b)** Sequence boundaries are indicated by numbers 1, 2, and 3, which are referred to in the text as B1, B2, B3. Blue 'B' and associated arrows note a sedimentary sequence that exists at U1545 but not at U1546. Those sediments seem to have infilled a relative seafloor depression that existed at the time that the boundary indicated by 'Y' was at the seafloor. Blue 'U' notes an angular unconformity at the B3 surface separating uplifted sediments at Site U1546 and sediments that were either deposited onto deformed sediment after the uplift or that were themselves deformed by the uplift; the later might explain the patchy coherency of layer-3 strata. The stratigraphy suggests that the sill intrusion occurred at some time between the ages of boundaries B3 and Y.

Figure S3. a) Depth migrated seismic image with locations and total drilled depths of Sites U1545 and U1546 indicated by vertical blue lines. Black box indicates the region shown enlarged in (b). **b)** Blue arrows indicate a wedge of sediments that is present at U1546 but not present at Site U1545. 'M' marks common mid-point (CMP) 850, just northwest of intense intrusion-related deformation of the overburden, where the correlation with Site U1546 is shown in Figure S3a.

Figure S4. *Caption in line with figure.*

Figure S5. *Caption in line with figure.*

Figure S6. Natural gamma-ray logs for Sites U1545 (left) and U1546 (right). The three main correlative intervals for these two sites, referenced to Site U1546, are 1) the upper interval extending from surface B3 at Site U1546 downward to the top of the 'wedge', 2) from the base of the 'wedge' to the top of the sill, and 3) from the bottom of the sill to the end of useful data on the Site U1545 log. The colored lines indicate the shifts in depth from the Site U1545 log to the Site U1546 log that align correlative peaks or troughs of the two logs (X-axis scale at the figure's bottom boundary); the average shift over the interval is indicated in meters. Variations in shift value with depth most likely reflect site-to-site differences in the thickness of individual stratal units. The difference in thickness correlated intervals is given in percent. Additional detail is provided in the text details.

Figure S7. *Tie points and discontinuities that define the site-to-site correlation between Sites U1545 and U1546.* Depth migrated seismic images for CMPs surrounding Site U1545 (left) and Site U1546 (right) are shown with the drill sites indicated as blue lines. The natural gamma ray (NGR) logs acquired at each site are overlain in black (see Figures S5 and S6 for scale). Numbered black segments crossing the blue borehole locations, with coincident cyan-colored horizontal extensions, are tie points connecting NGR signals that are common to each drill site, with reflectivity signals generally also common. Magenta lines mark the discontinuities in the

stratigraphic record between the two sites. The upper magenta line at U1545 is paired with the upper two magenta lines at U1546, together defining the stratigraphic discontinuity presented by the 'wedge' of sediments that are present at U1546 but absent at U1545 (see Figure S3). Similarly, the lower magenta line at U1545 is paired with the lower two magenta lines at U1546, together defining the discontinuity presented by the intruded sill at Site U1546. This set of 24 tie points plus 2 discontinuities defines the site-to-site correlation used to align the NGR profiles shown in Figure S8 and, importantly, to map Site U1545 core samples to Site U1546 over the 1.75- to 2.06-km depth interval.

Figure S8. *Expanded view of the correlated NGR logs referenced to depth at Site U1546.* The Site U1546 log is shown in brown and the Site U1545 log in black. Visual inspection shows that the correlation at all depth is excellent to very good, including the correlation beneath the sill. The NGR log for Site U1546 has values substantially higher over the lower correlative interval than those for Site U1545 over that interval. The increase in NGR values at U1546 most likely reflects increased density of those sediments due to compaction [e.g., Nobes et al., 1992].

Figure S9. *Correlated density logs referenced to depth at Site U1546.* As for Figure S8, the Site U1546 density log is shown in brown and the Site U1545 log in black. The U1545 density log has been shifted based on the correlation defined by the NGR logs and seismic data, shown in detail in Figure S7. Visual inspection shows that the correlation at all depth is excellent to very good, including the correlation beneath the sill. As for the NGR log correlation, the gap in U1545 correlated data from 1.90-1.911 (correlated depth) corresponds to the sedimentary wedge indicated in Figures S3 and S4. The gap in the density log from 1.938-1.955 mbsf (correlated depth) represents an actual gap in the U1545 density log data. This gap has been filled with the value indicated by the green line (1.685 gm/cm^3), which is median value from the U1545 density over the interval indicated, 1.920-2.055 mbsf (correlated depth). Blue dots are density measurements made on core samples from U1545, which are consistent with the log data and support the chosen median value as a reasonable.

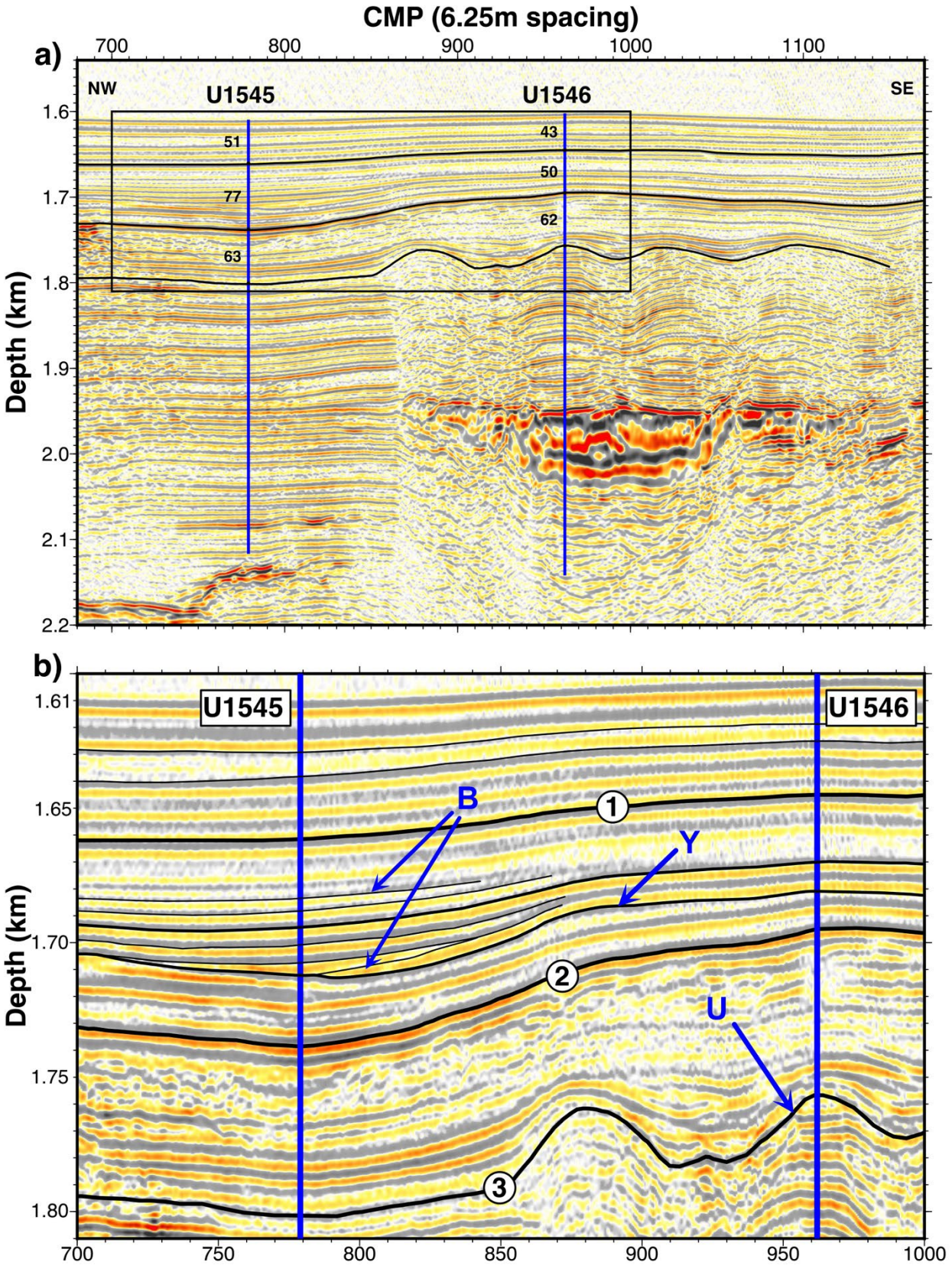
CMP (6.25m spacing)
a)
NW
SE
U1545
U1546
51
77
63
43
50
62
Depth (km)
b)
U1545
U1546
B
Y
U
1
2
3
Depth (km)

Figure S2

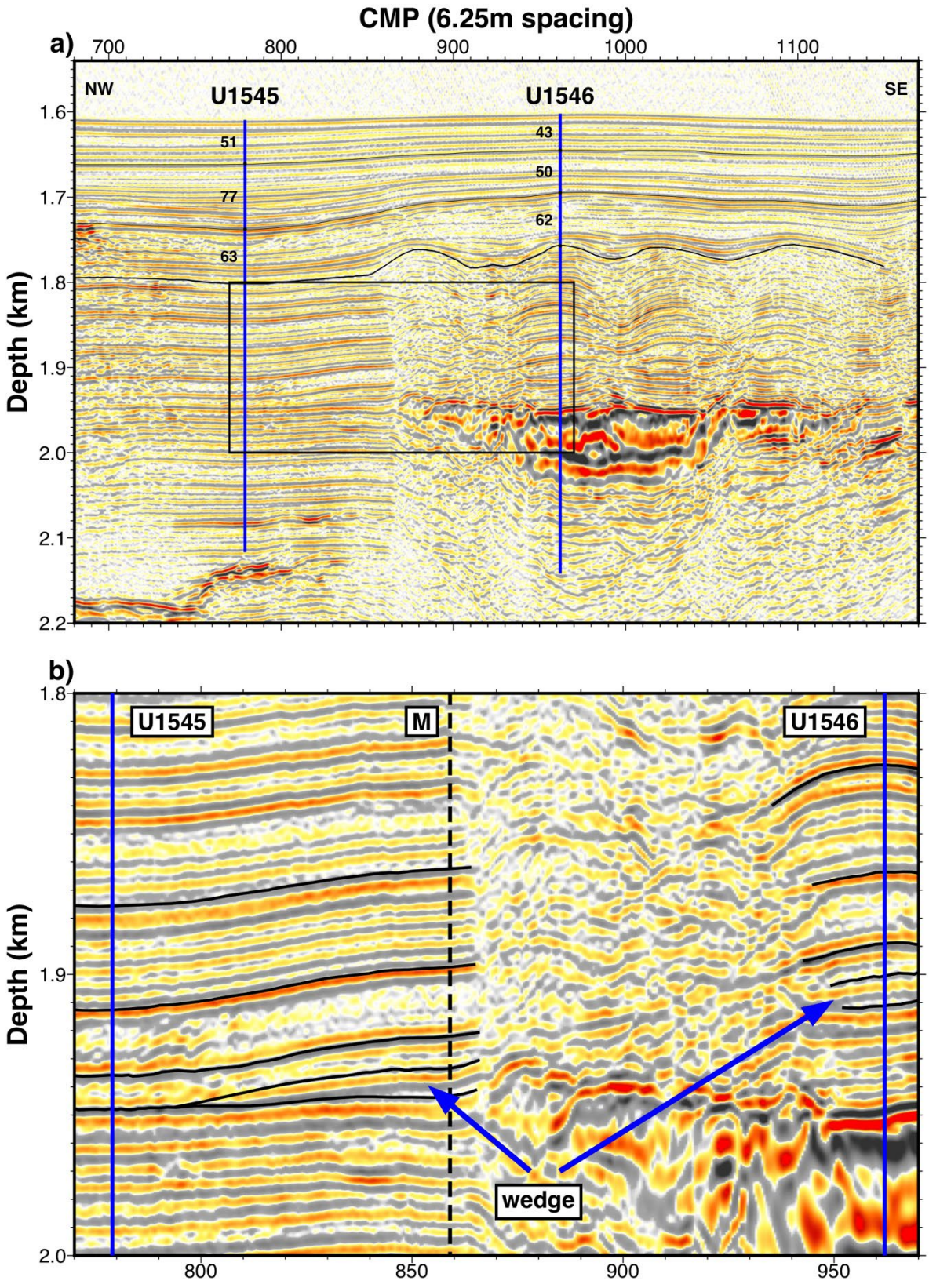
a)
CMP (6.25m spacing)
700
800
900
1000
1100
NW
SE
U1545
U1546
51
77
63
43
50
62
Depth (km)
1.6
1.7
1.8
1.9
2.0
2.1
2.2
b)
U1545
M
U1546
wedge
Depth (km)
1.8
1.9
2.0
800
850
900
950

Figure S3

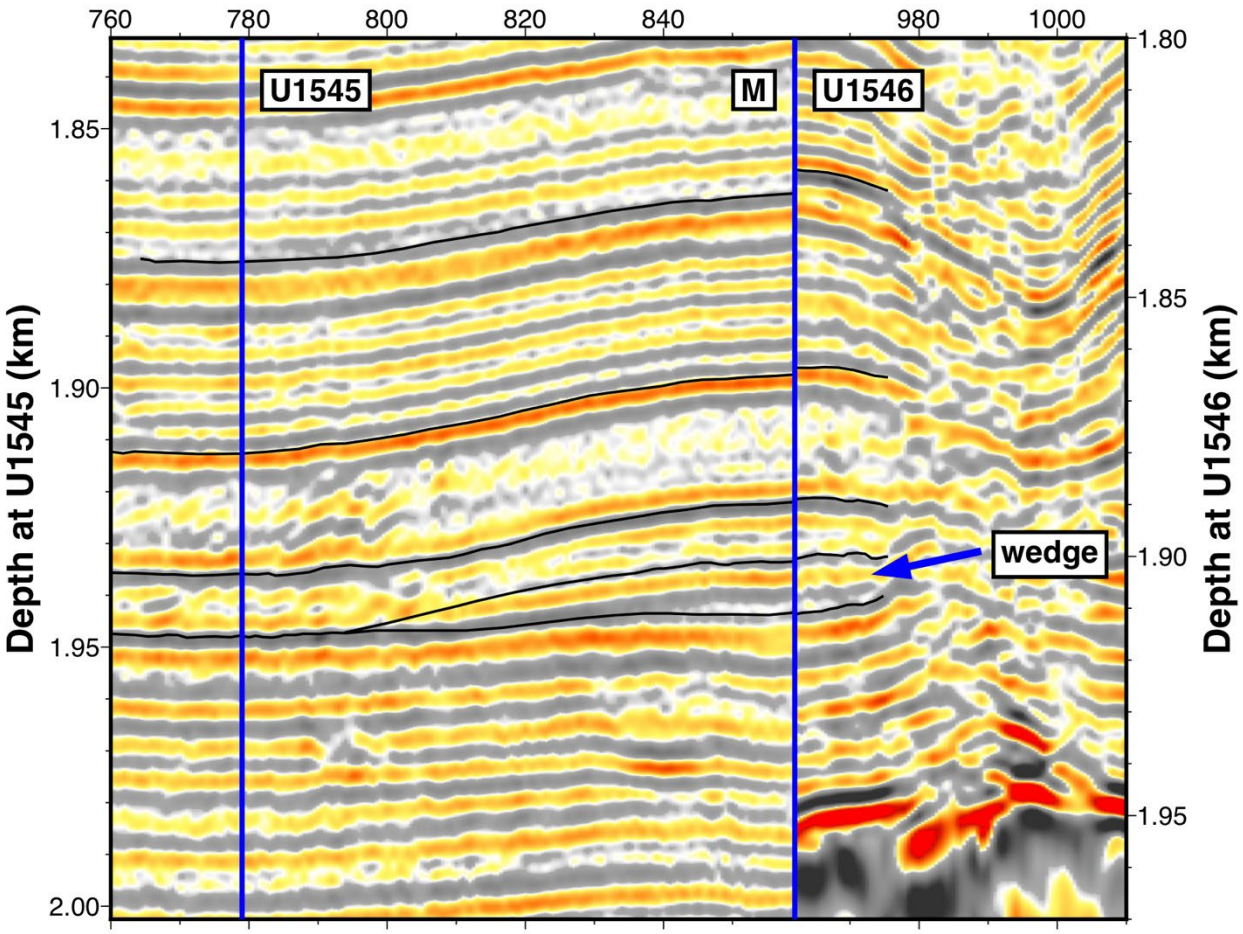

Figure S4

Figure S4. Stratigraphic correlation at 'M' (CMP 850) and U1546 (CMP 962) made by shifting the entire seismic section on the U1545 side of M upward in order to tie the wedge strata at the two CMPs. The 'wedge' sediments are well correlated from 'M' to Site U1546 and are absent at Site U1545. A distinct, common pattern of seismic stratigraphic units is also observed on either side of 'M', though the amount of 'shift' needed to tie common stratal units varies as a function of depth, indicating lateral changes in thickness within individual units.

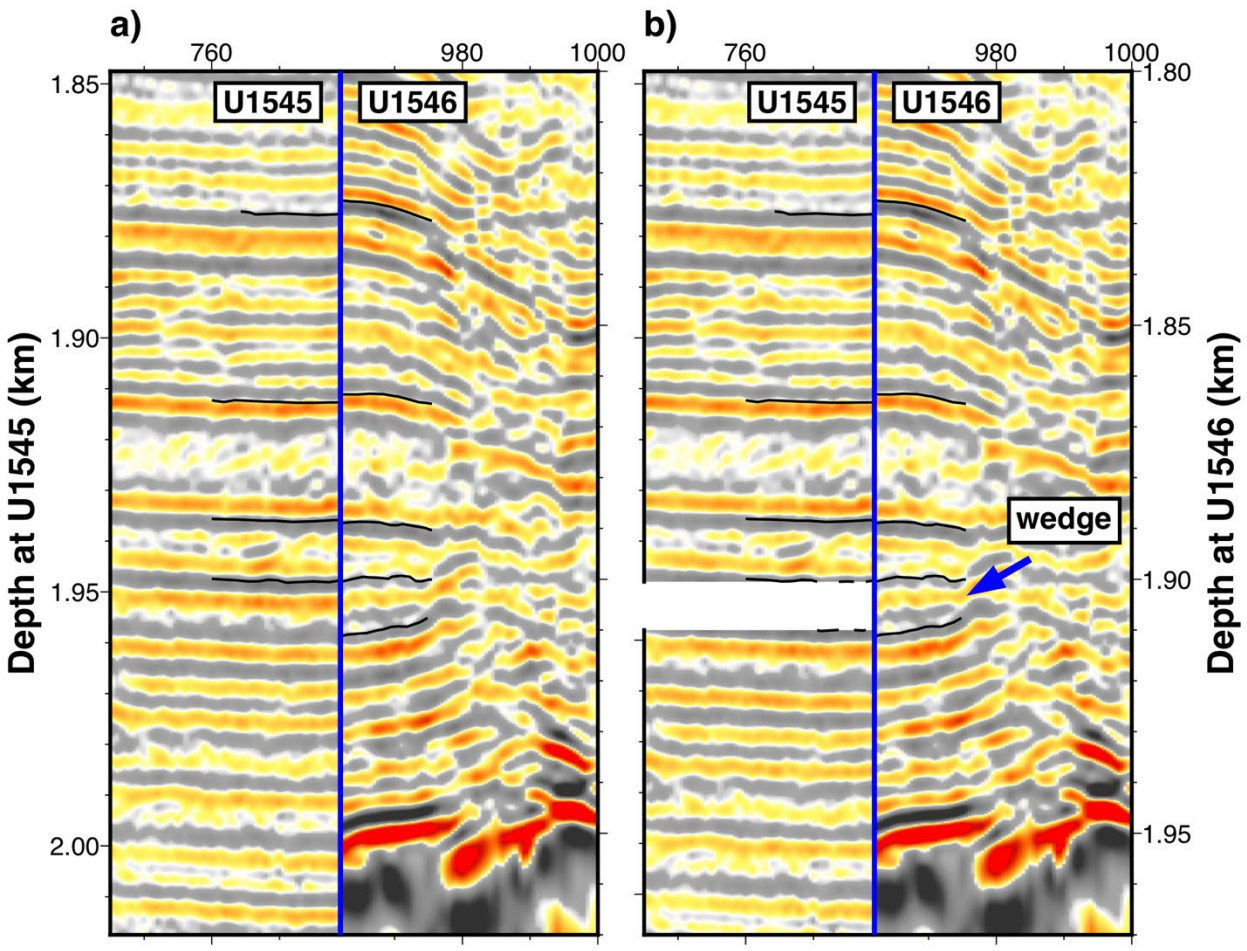

Figure S5

Figure S5. a) Stratigraphic correlation at Site U1545 (CMP 779) and U1546 (CMP 962) made by shifting the entire seismic section on the U1545 side upward in order to tie the wedge strata at the two CMPs. This tie is visually acceptable, but it is inconsistent with the stratigraphic observation of the wedge shown in Figure S3, and it is also inconsistent with the natural gamma ray logs. **b)** As in (a), but the sediments on the U1545 side have been shifted down below the upper tie point with the wedge sediments present at U1546.

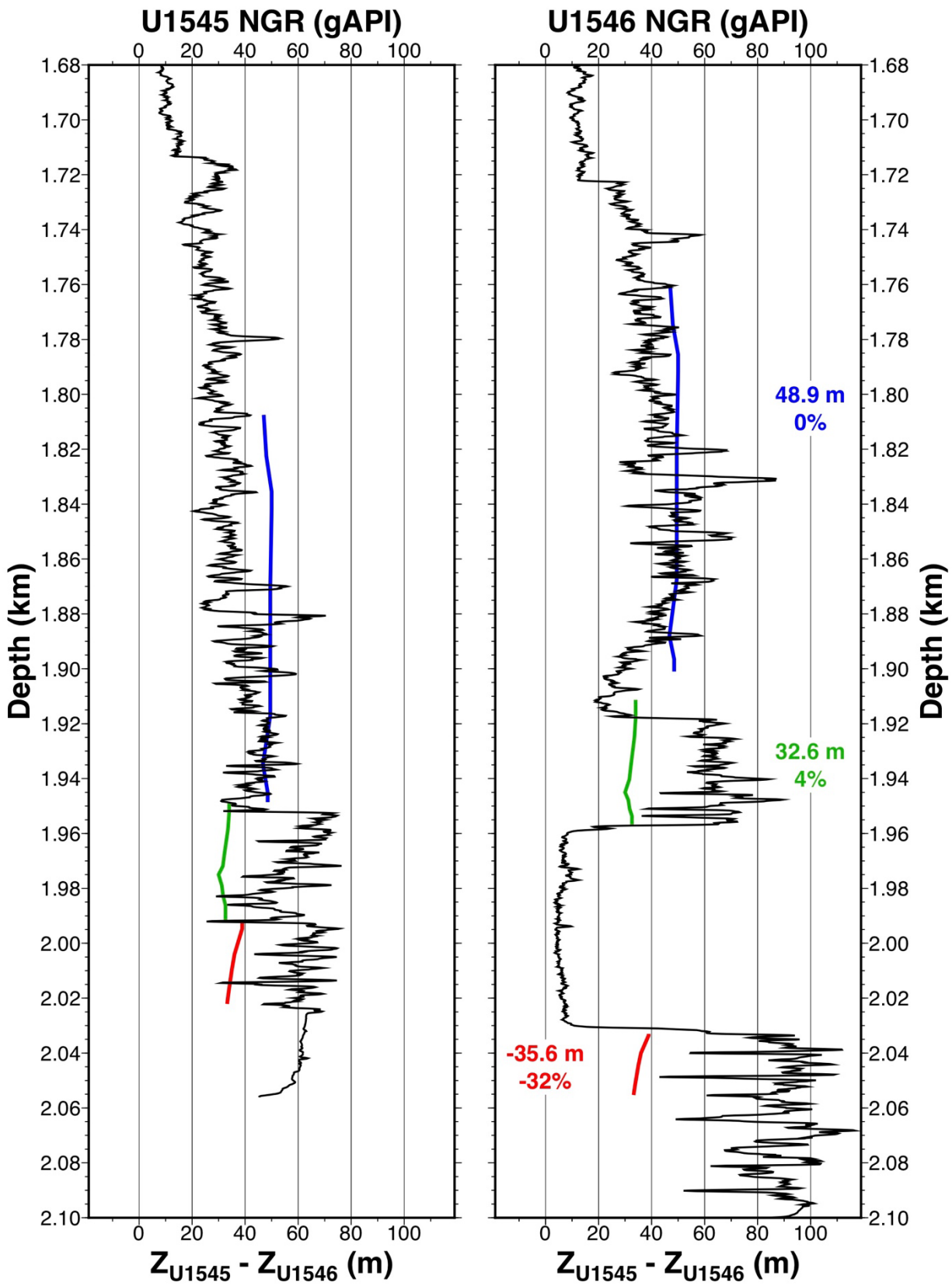
U1545 NGR (gAPI)
U1546 NGR (gAPI)
0
20
40
60
80
100
1.68
1.70
1.72
1.74
1.76
1.78
1.80
1.82
1.84
1.86
1.88
1.90
1.92
1.94
1.96
1.98
2.00
2.02
2.04
2.06
2.08
2.10
Depth (km)
48.9 m
0%
32.6 m
4%
-35.6 m
-32%
Z_{U1545} - Z_{U1546} (m)

Figure S6

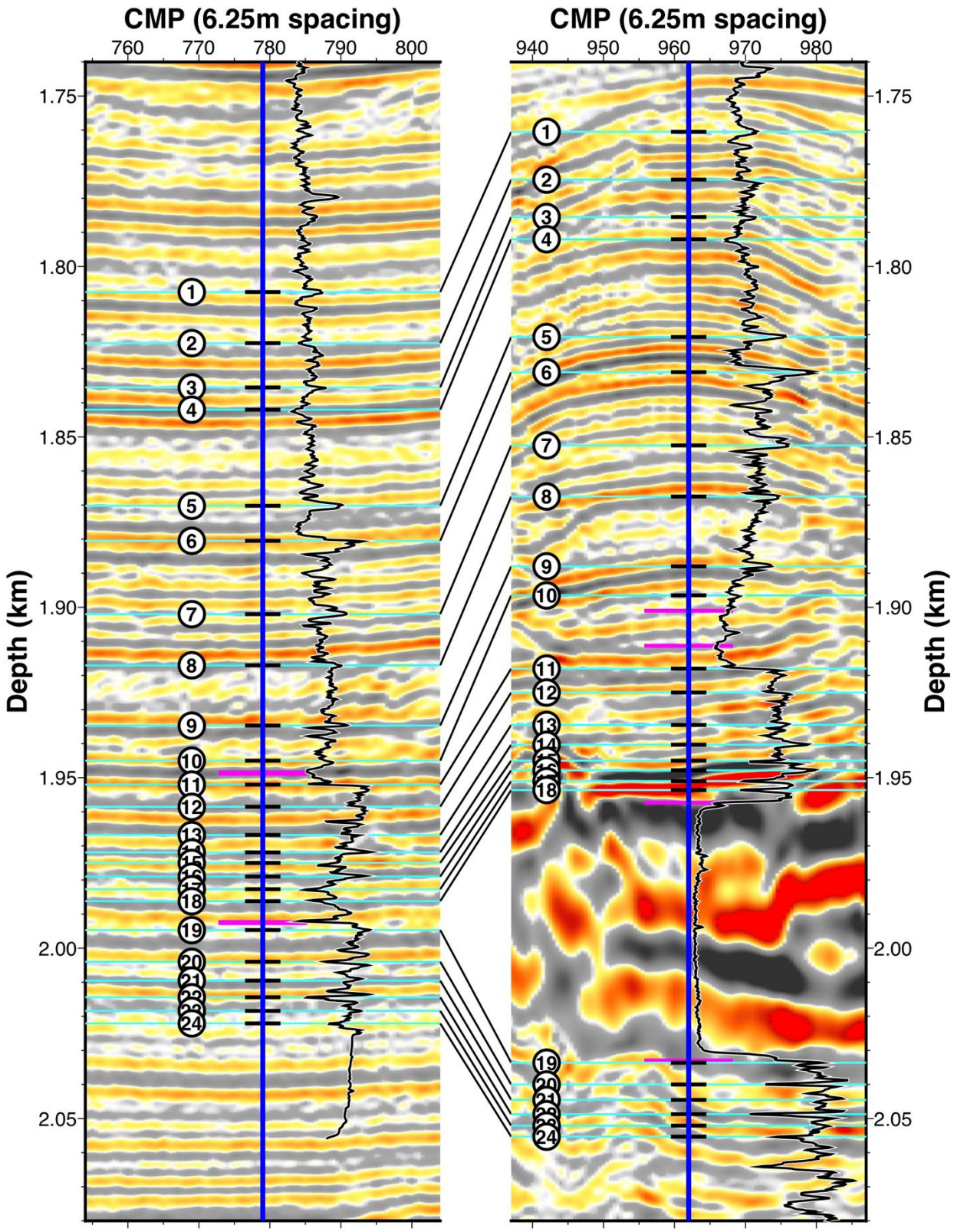
CMP (6.25m spacing)
760
770
780
790
800
CMP (6.25m spacing)
940
950
960
970
980
Depth (km)
1.75
1.80
1.85
1.90
1.95
2.00
2.05
Depth (km)
1.75
1.80
1.85
1.90
1.95
2.00
2.05

Figure S7

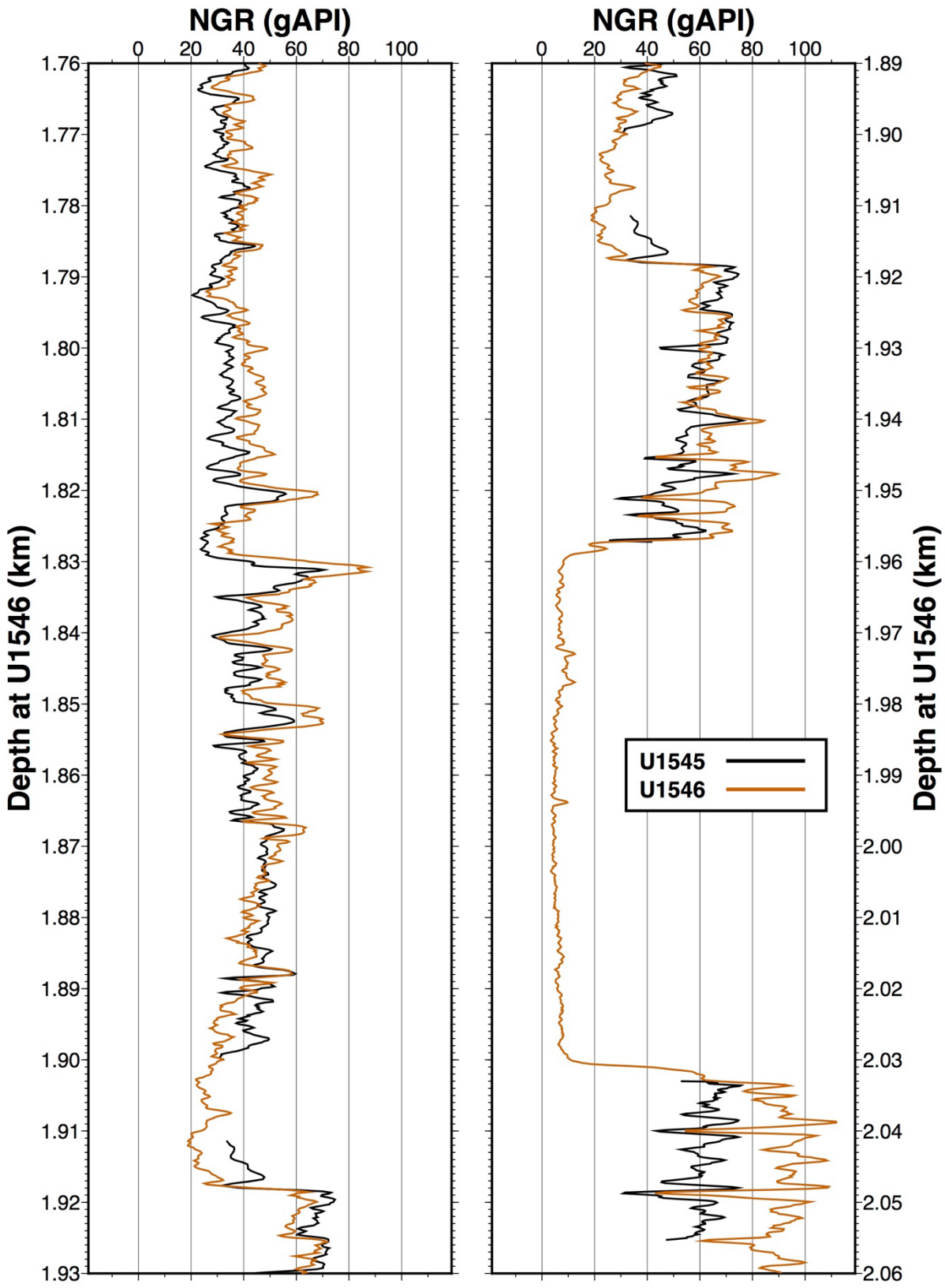
NGR (gAPI)
0
20
40
60
80
100
Depth at U1546 (km)
1.76
1.77
1.78
1.79
1.80
1.81
1.82
1.83
1.84
1.85
1.86
1.87
1.88
1.89
1.90
1.91
1.92
1.93
1.89
1.90
1.91
1.92
1.93
1.94
1.95
1.96
1.97
1.98
1.99
2.00
2.01
2.02
2.03
2.04
2.05
2.06
U1545
U1546

Figure S8

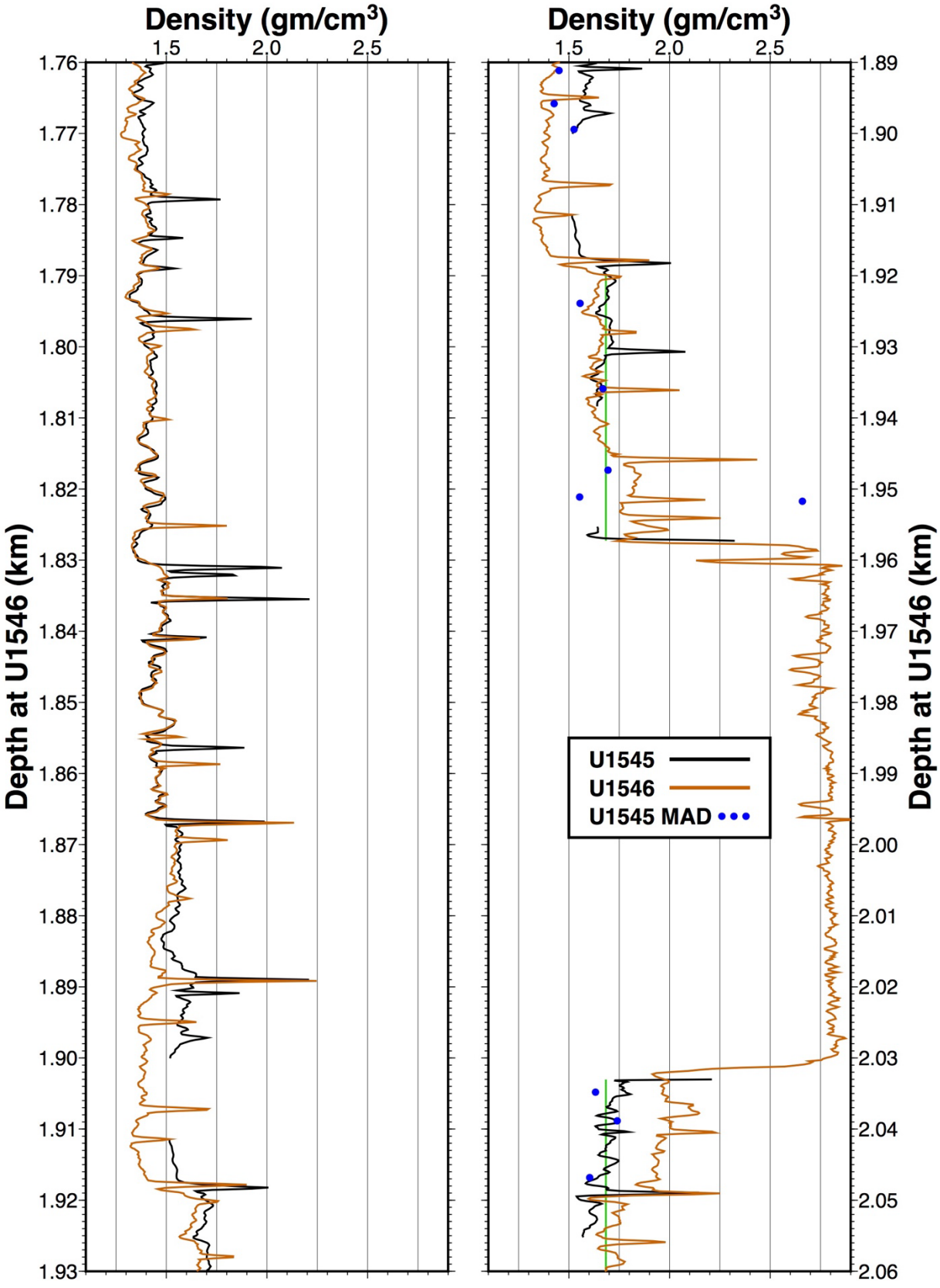
Density (gm/cm3)
1.5
2.0
2.5
Depth at U1546 (km)
1.76
1.77
1.78
1.79
1.80
1.81
1.82
1.83
1.84
1.85
1.86
1.87
1.88
1.89
1.90
1.91
1.92
1.93
Density (gm/cm3)
1.5
2.0
2.5
Depth at U1546 (km)
1.89
1.90
1.91
1.92
1.93
1.94
1.95
1.96
1.97
1.98
1.99
2.00
2.01
2.02
2.03
2.04
2.05
2.06
U1545
U1546
U1545 MAD

Figure S9